Improving Arctic sea-ice thickness estimates with the assimilation of CryoSat-2 summer observations

Chao Min[1,2], Qinghua Yang[1], Hao Luo[1], Dake Chen[1], Thomas Krumpen[2], Nabir Mamnun[2], Xiaoyu Liu[2], and Lars Nerger[2]

[1]School of Atmospheric Sciences, Sun Yat-sen University, and Southern Marine Science and Engineering Guangdong Laboratory (Zhuhai), Zhuhai, China.

[2]Alfred Wegener Institute, Helmholtz Centre for Polar and Marine Research, Bremerhaven, Germany.

[*]Address correspondence to: yangqh25@mail.sysu.edu.cn

Abstract

Rapidly shrinking Arctic sea ice has had significant impacts on the Earth system. Therefore, reliably estimating the Arctic sea-ice thickness (SIT) using a combination of available observations and numerical modeling is urgently needed. Here, for the first time, we assimilate the latest CryoSat-2 summer SIT data into a coupled ice-ocean model. In particular, an incremental analysis update scheme is implemented to overcome the discontinuity resulting from the combined assimilation of biweekly SIT and daily sea-ice concentration (SIC) data. Along with improved estimates of sea-ice volume, our SIT estimates corrected the overestimation of SIT produced by the reanalysis that assimilates only SIC in summer in areas where the sea ice is roughest and experiences strong deformation, e.g., around the Fram Strait and Greenland. This study suggests that the newly developed CryoSat-2 SIT product, when assimilated properly using our approach, has great potential for Arctic sea ice simulation and prediction.

Keywords

Arctic sea ice; Sea ice thickness; Data assimilation; Incremental analysis update; CryoSat-2

1. Introduction

Coinciding with the Arctic warming ratio that is four times that of the global average (Chylek et al., 2022; Rantanen et al., 2022), Arctic sea ice has sharply declined during the satellite era (Kwok, 2018; Stroeve & Notz, 2018). Substantial sea ice loss has significantly influenced the Earth system (Bailey et al., 2021; Cohen et al., 2021; Liu et al., 2022; Qi et al., 2022). For instance, the Arctic sea ice reduction has been linked to some extreme events at middle and lower latitudes (Bailey et al., 2021; Cohen et al., 2021; Liu et al., 2022). Although the ongoing decline has made commercial trans-Arctic transit more feasible in the summer, the changing and mobile sea ice impacts maritime activities (e.g., Eicken, 2013; Min, et al., 2022). For instance, local variations in the sea-ice thickness (SIT) can affect the safety and route planning of maritime navigators. Consequently, there is a great need for and interest in reliable measurements, simulations and forecasts of Arctic sea ice.

Sophisticated year-round sea-ice concentration (SIC) monitoring has been developed for several decades (e.g., Comiso et al., 1997; Lavergne et al., 2019; Spreen et al., 2008). Satellite sea ice data such as those derived from the Soil Moisture and Ocean Salinity (SMOS, Kaleschke et al., 2012; Tian-Kunze et al., 2014) and CryoSat-2 (Laxon et al., 2013; Ricker et al., 2014) products record the ice thickness over several years, but processing challenges in summer have resulted in the availability of only winter observations. Recently, a pan-Arctic summer SIT product derived from CryoSat-2 has become available (Landy et al., 2022). The most recent CryoSat-2 observations not only offer a look at pan-Arctic SIT from the perspective of satellite remote sensing year-round but also provide opportunities for constructing a more reliable SIT reanalysis by assimilating these data into dynamical models and generating sea-ice forecasts (Landy et al., 2022).

Data assimilation can strongly enhance sea-ice estimates because the model initialization can be adjusted and the model state can be continuously constrained to reality by integrating new observations (Blockley & Peterson, 2018; Day et al., 2014; Massonnet et al., 2015). The assimilation of winter SIT, for instance, can provide improved initial conditions for the summer season and hence has the potential to lower uncertainty in both sea-ice estimates and forecasts (e.g., Blockley & Peterson, 2018; Day et al., 2014; Mignac et al., 2022; Xie et al., 2018; Yang et al., 2014; Yang et al., 2019). In particular, to improve the ice-thickness estimates, a year-round Combined Model and Satellite Thickness (CMST) reanalysis has been developed by assimilating the CryoSat-2 and SMOS thickness data throughout the freezing season (Mu, Losch, et al., 2018). Although the CMST has been systematically evaluated and widely used (e.g., Li et al., 2022; Min et al., 2019; Min et al., 2021; Mu, Losch, et al., 2018; Zhou et al., 2021), the SIT is corrected only indirectly in summer through the positive covariance between SIC, which is assimilated, and SIT, which is not assimilated during the summer months. Moreover, the weekly mean SIT from CryoSat-2 is simply assimilated every day of the week during the cold season (Mu, Losch, et al., 2018; Mu, Yang, et al., 2018), which may introduce unrealistic "jumps" at the transition points between different weeks and seasons (i.e., winter-summer and summer-winter). To date, there have not been studies on the impacts of and approaches for assimilating satellite-based summer SIT. Given the current availability of summer SIT data, we conducted a data assimilation experiment by simultaneously assimilating summer SIC and SIT.

This study aimed to explore whether the assimilation of CryoSat-2 summer SIT data can better constrain modeled SIC and SIT and thus improve sea ice estimates. We applied an incremental analysis update (IAU) scheme for CryoSat-2 summer SIT assimilation to ensure the physical development of sea ice volume (SIV) and SIT given that CryoSat-2 observations were available only at a lower biweekly time interval than the daily SIC observations. We further compared our outputs with those of the CMST and different independent data to assess the overall improvement resulting from assimilating summer SIT.

2. Materials and Methods

2.1 Observations for data assimilation

The pan-Arctic, year-round CryoSat-2 SIT dataset has been generated by combining deep learning radar waveform classification with numerical radar simulation (Landy et al., 2022). In summary, a one-dimensional convolutional neural network has been applied to classify leads from sea-ice returns in radar altimeter waveform (Dawson et al., 2022). A series of numerical waveform simulations based on the Facet-Based Echo Model (Landy et al., 2020;

Landy et al., 2019), which integrates melt ponds, are then used to calibrate a radar range bias that causes the CryoSat-2 freeboards to be underestimated. The SIT is derived from CryoSat-2 radar freeboards, assuming hydrostatic equilibrium and accounting for snow loading, with snow depth and density estimates obtained from the MERRA-2 version of SnowModel-LG (Liston et al., 2021). The innovative dataset provides the SIT and its uncertainty with a temporal resolution of 15 or 16 days and a spatial resolution of 80 km. Nevertheless, large uncertainties remain close to the coast of northern Greenland, the Canadian Arctic Archipelago and the Fram Strait when compared to airborne electromagnetic thickness observations (Landy et al., 2022). More details about the data processing can be found in Dawson et al. (2022) and Landy et al. (2022).

The SIC data used in this study are computed at the French Research Institute for Exploitation of the Sea (IFREMER) and reprocessed by the Integrated Climate Data Center. Together with the ARTIST (Arctic Radiation and Turbulence Interaction STudy) Sea Ice algorithm (Kaleschke et al., 2001; Spreen et al., 2008), this SIC dataset is derived from brightness temperatures measured with the 85-GHz Special Sensor Microwave/Imager (SSM/I) and/or Special Sensor Microwave/Imager Sounder (SSM/IS) channels. A 5-day median filter is used to reduce unrealistic short-term SIC variations resulting from the influence of weather (Kern et al., 2010). The spatial resolution of the daily SIC data is 12.5 km.

2.2 Reference observations

The SIC observations, which are processed by the National Aeronautics and Space Administration (NASA) Team algorithm and distributed by the National Snow and Ice Data Center (NSIDC, DiGirolamo et al., 2022), are processed into the sea-ice extent (SIE) prior to assessing the SIEs estimated by CMST and our experiments. This reference SIC dataset is used to ensure that we are not assimilating and testing against the same observations. Notably, the SIC dataset derived from the NASA Team algorithm distributed by the NSIDC and the SIC dataset computed at the IFREMER are both derived from the same brightness temperatures/emissivity measured by the Special Sensor Microwave/Imager (SSM/I) and/or the Special Sensor Microwave/Imager Sounder (SSM/IS), which prevents them from being considered independent data. The two SIC observations are, however, retrieved using different algorithms. Therefore, we can assume that the NSIDC SIC data are sufficiently different and can be utilized as reference observations.

The in situ observations of SIT are limited to a very small area, with nearly no observations available in the Central Arctic region. To validate the SIT results, we use a set of independent fixed mooring and airborne SIT observations (see Fig. 1 for geographic locations of surveys and deployment positions). Sea ice drafts from May 23 to September 30, 2016, were obtained from upward-looking sonars (ULSs) provided by the Beaufort Gyre Experiment Program (BGEP). The data from the three different moorings are hereafter referred to as BGEP_A, BGEP_B and BGEP_D. According to Melling et al. (1995), the error associated with ULS sea ice draft observations is approximately 0.1 m. Additionally, draft data from May 23 to August 8, 2016, collected by the Alfred Wegener Institute (AWI) using an acoustic Doppler current profiler (ADCP) in the western Laptev Sea area, are used. Per Belter et al. (2021), the uncertainties in the hourly observations are relatively high (±0.96 m) but consistent. To simplify the comparison between the model SIT and observations, the observed sea ice draft is converted to thickness by multiplying it by a factor of 1.1 (Nguyen et al., 2011).

In addition to the moored observations, SIT from airborne electromagnetic surveys conducted by the Alfred Wegener Institute (AWI) in the Fram Strait and northern Greenland (Krumpen et al., 2019) are used as a reference dataset for our model results. The applied surveys were conducted between July 24 and August 1, 2016, during the IceBird campaign. For more details on the methodology, we refer to Krumpen et al. (2020). According to Pfaffling et al. (2007), airborne observations are estimated to have an uncertainty of ±0.1 m over flat ice, although the accuracy may be affected by the presence of melt ponds. As the footprint of airborne measurements is in the range of tens of meters, all airborne electromagnetic ice thicknesses are averaged onto the CryoSat-2 grids for comparison, following Landy et al. (2022). As the numerical model uses the effective/mean ice thickness (volume over an area), all field observations are multiplied by the local NSIDC SIC to obtain the observed mean thickness to facilitate comparison between the model and observations, following Yang et al. (2015). Because the in situ ULS/ADCP measures SIT on a subkilometer scale while the modeled SIT is on a multikilometer scale, there are some limitations to comparing the modeled SIT with these point measurements from the observations. However, by averaging the values over a timespan of one day, we assume the ULS/ADCP samples over a wide range of the ice thickness distribution, as floes drift over the mooring. Following previous studies (e.g., Yang et al., 2014; 2015), this study does not attempt to quantify these uncertainties.
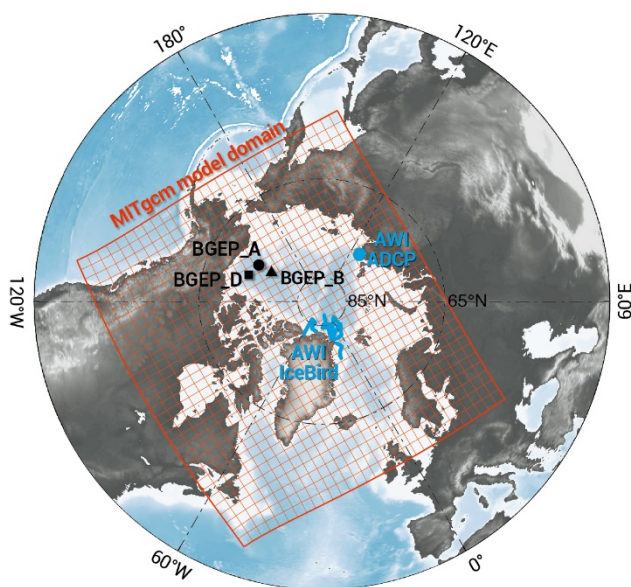
Fig. 1. The MITgcm model grid is shown in an orange net plotted at 12 model grid points. The independent observations used to validate CryoSat-2, the Combined Model and Satellite Thickness (CMST) and the analysis field (ANA) are presented as extra-large blue dots for the two Alfred Wegener Institute (AWI) acoustic Doppler current profiler (ADCP) sensor deployments, as blue lines for the AWI airborne surveys (IceBird), and as a black dot, triangle and square for the A, B and D moorings, respectively, of the Beaufort Gyre Exploration Program (BGEP). The blue dots for the two AWI ADCPs (Vilk1-14 and Vilk3-14) overlap due to their proximity.

2.3 Sea-ice data assimilation system

The data assimilation system is further developed based on the CMST system. For example, the Massachusetts Institute of Technology general circulation model (MITgcm, Marshall et

al., 1997) and the Parallel Data Assimilation Framework (PDAF, Nerger & Hiller, 2013) are employed. Sea ice dynamics use a viscous plastic rheology (Hibler, 1979; Zhang & Hibler, 1997), with a one-layer, zero-heat capacity formulation applied in thermodynamics (Parkinson & Washington, 1979; Semtner, 1976). Fifty vertical model layers are used in the ocean model, with 28 layers located in the top 1000 m. An Arakawa C grid with a variable horizontal resolution and an average spacing of 18 km is used to discretize both the ocean and sea ice models. The experiments are based on a regional MITgcm configuration with open boundaries located around 55°N in the Atlantic and Pacific (Losch et al., 2010; Nguyen et al., 2011). Fig. 1 depicts the model domain with an orange mesh.

As with earlier data assimilation studies (e.g., Mu, Losch, et al., 2018; Mu, Yang, et al., 2018; Yang et al., 2015), the coupled ice-ocean model is driven by atmospheric ensemble forecasts generated by the UK Met Office (UKMO) Ensemble Prediction System (EPS) and accessible from The Observing System Research and Predictability Experiment (THORPEX) Interactive Grand Global Ensemble archive (TIGGE) (Bowler et al., 2008; Park et al., 2008) to incorporate flow-dependent uncertainty in atmospheric forcing. Eleven sets of perturbed forecasts are employed to force an ensemble of eleven model states. Details about the atmospheric data processing can be found in previous studies (Mu, Losch, et al., 2018; Yang et al., 2015).

By using the multivariate covariances between ice concentration and thickness, Yang et al. (2015, 2016) found that assimilating the summer SIC improved the forecast and estimate of the summer SIT. Based on this, Mu, Losch, et al. (2018) developed the year-round CMST reanalysis. However, uncertainties remain in the heavily deformed and ridged sea ice region. Thus, we conduct this study to further improve the SIT estimates. For easy comparison with the previously-developed CMST reanalysis, which assimilates only the IFREMER SIC during summer, following Mu, Losch, et al. (2018), the IFREMER SIC and CryoSat-2 SIT are assimilated into the ice-ocean model by using the local error-subspace transform Kalman filter (LESTKF) coded in PDAF (Nerger & Hiller, 2013; Nerger et al., 2012). The LESTKF, a local formulation of ESTKF, is a highly efficient ensemble Kalman filter with very high-dimensional models (Nerger et al., 2012). In particular, the ESTKF can be used with a deterministic minimum transformation, which allows the use of particularly small ensembles. The SIC and SIT obtained from the forecast fields are stored together in the state vector. Then, at each analysis step, the LESTKF is used to correct the state vector by only accounting for the sea-ice data observed within a 126 km radius of each model point (Mu, Losch, et al., 2018; Yang et al., 2015). The observations within the radius are weighted with distance from the grid point by a quasi-Gaussian weight function (Gaspari & Cohn, 1999). The model uncertainties are calculated from the ensemble of model states driven by the UKMO ensemble atmospheric forcing (Mu, Losch, et al., 2018; Yang et al., 2015). The observation error for SIC is set as a constant value of 0.25. This choice is based on sensitivity experiments in our previous studies (e.g., Mu, Losch, et al., 2018; Yang et al., 2016) and accounts for the representation error. For the SIT observations, variable observation errors provided with the CryoSat-2 dataset are used; for an example of SIT uncertainty during summer 2016, see Fig. 2.
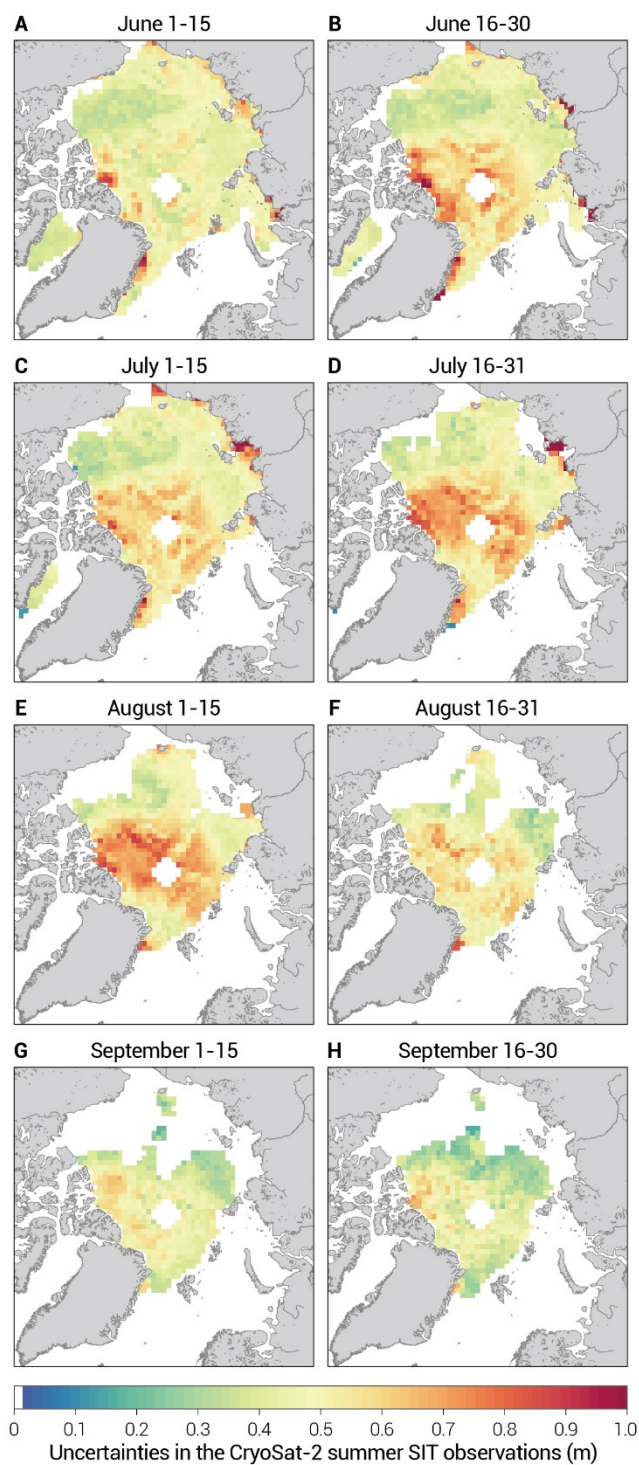
Fig. 2. Uncertainties in the CryoSat-2 summer sea-ice thickness (SIT) observations. Figures in the left panel (a, c, e, and g) and the right panel (b, d, f, and h) are uncertainty maps of CryoSat-2 summer SIT data for the first and second halves, respectively, of June, July, August, and September 2016.

For consistent pan-Arctic temporal and spatial coverage, CryoSat-2 SIT data are available twice a month at intervals of 15 or 16 days (Landy et al., 2022; Lawrence et al., 2021). Therefore, the forecast interval between the analysis steps is excessively long when directly assimilating CryoSat-2 data. The sparse analysis step typically creates unrealistically large

"jumps" in the evolution of sea ice, leading to an unnatural development of SIV (Fig. A1). For forecasting systems that need daily updates, direct assimilation of these data is therefore inappropriate. Hence, an IAU strategy similar to those of previous studies (Bloom et al., 1996; Lellouche et al., 2013; Ourmières et al., 2006) is implemented to obtain smoother evolutions of sea ice. The IAU is applied only for the CryoSat-2 summer observations while assimilating SIC observations instantaneously. The IAU scheme developed in this study is schematically shown in Fig. 3. In brief, this IAU scheme is cycled with a combination of 7-/8-day runs and rerun over 15 or 16 days. For this, we first execute a 7-/8-day assimilation run, which assimilates daily SIC, initialized from the previous state at the beginning (light blue dots in Fig. 3) of each period of the biweekly mean CyoSat-2 SIT data. At the end of this first run (bright blue squares in Fig. 3), the CryoSat-2 SIT is assimilated. The total SIT increment obtained at the analysis step is not immediately applied but divided by 15 or 16, according to the time span of the assimilated CyoSat-2 SIT, and stored for the IAU to perform daily updates. Finally, for a 15-/16-day assimilation experiment, we restart our system at the initial time of the first 7-/8-day run (light blue dots in Fig. 3) and assimilate the daily SIC while also incorporating the daily SIT increment into the data assimilation system. This cycle is repeated during the whole assimilation cycle. This approach allows us to assimilate the rather infrequent biweekly summer SIT data in combination with the daily SIC data while ensuring a gradual development of the sea ice fields over time.
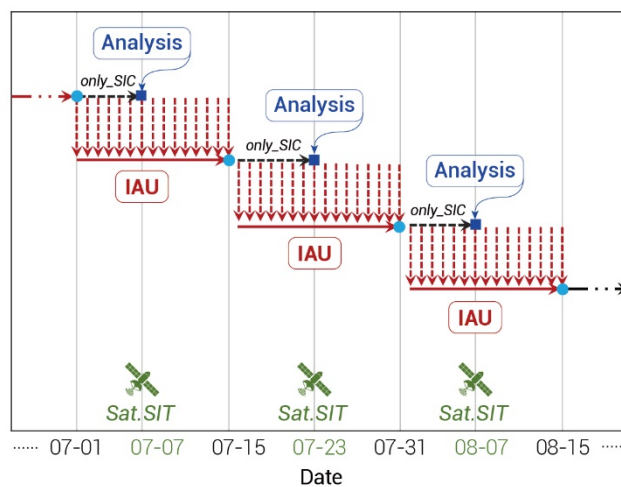
Fig. 3. A schematic illustration of the incremental analysis update (IAU) approach implemented in our data assimilation system. The light blue dots represent the initial states for modeled summer sea ice at the beginning of the 15-day or 16-day period for biweekly mean CyoSat-2 sea-ice thickness (SIT), while the dark blue squares are for the analysis fields with SIC and SIT assimilation. The dates in green font denote the dates of available CyoSat-2 SIT data. The dashed arrows represent the daily SIT increment in the IAU approach.

2.4 Experimental design

In the beginning of 2016, a record-low monthly SIE was experienced, but the summer extent exceeded most seasonal forecasts (Petty et al., 2017; Petty et al., 2018). Due to the unconsolidated summer ice cover in 2016, modeling and forecasting sea ice conditions during this summer are expected to be exceptionally challenging (Petty et al., 2017; Petty et al., 2018). To test our system, which has been newly developed with the IAU scheme, we carried out a case study from May 23 to September 30, 2016. Given that CMST data are already well validated and applied (e.g., Li et al., 2022; Min et al., 2019; Min et al., 2021;

Mu, Losch, et al., 2018; Zhou et al., 2021), following Yang et al. (2019), restart files from this retrospective simulation (CMST) are used as the initial ice-ocean conditions for the data assimilation experiments.

3. Results

The spatial distributions of summer SIT are displayed in Figs. 4a-4c. Overall, assimilating the summer SIT leads to a better agreement of the SIT and SIV estimated from our thickness analysis field (hereafter, ANA) with that from CryoSat-2 compared to CMST, which only assimilates SIC during the summer. Compared to that of CMST, the SIT distribution from ANA is more similar to that from CryoSat-2. Fig. 4d further illustrates the differences between the absolute value of ANA minus CryoSat-2 and the absolute value of CMST minus CryoSat-2, showing that ANA has been significantly improved. The overestimation of the ice thickness by CMST is corrected, particularly in the Fram Strait and in the Arctic Ocean on the northern coast of the Canadian Arctic Archipelago and Greenland. These are regions where the sea ice experiences stronger deformation and the ice surface is roughest (Farrell et al., 2020; Kwok, 2015).

Root-mean-square error (RMSE), mean bias, and the correlation coefficient, whose calculation methods are described in Appendix A2, are used to quantify the comparisons between the CMST, ANA, and observations. Our results demonstrate relatively strong agreement with the observed SIE (Fig. A2) and SIV (Fig. 4e) during the entire summer season, both during the ice melting phase and freezing period (mid-September). The correlation coefficients for SIV between the ANA/CMST and the observations are nearly equal (0.97 between the ANA and CryoSat-2 data). In relation to the SIV calculated by CMST and ANA, the RMSEs decrease from 2.43×10^3 km^3 to 1.97×10^3 km^3, demonstrating that the estimates for SIV are improved. Owing to the lack of assimilating summer SIT, the initial condition from CMST still shows a significant initial error in estimating SIV. In addition, we suppose there are two reasons why the SIV in early summer, as estimated by ANA, is much closer to the CMST than to the CryoSat-2 data. First, the data assimilation system needs a certain amount of time to spin up before leading to consistent improvements (Mu, Yang, et al., 2018). Second, around the early summer, CryoSat-2 exhibits substantially higher uncertainty (Fig. 2) than does the model state, making the ANA results closer to those of the model state. Note that from the end of June, as the assimilation process moves forward, the observational information is weighted more to correct the model state based on the model and observation error covariances, leading to a stable correction of the SIT.
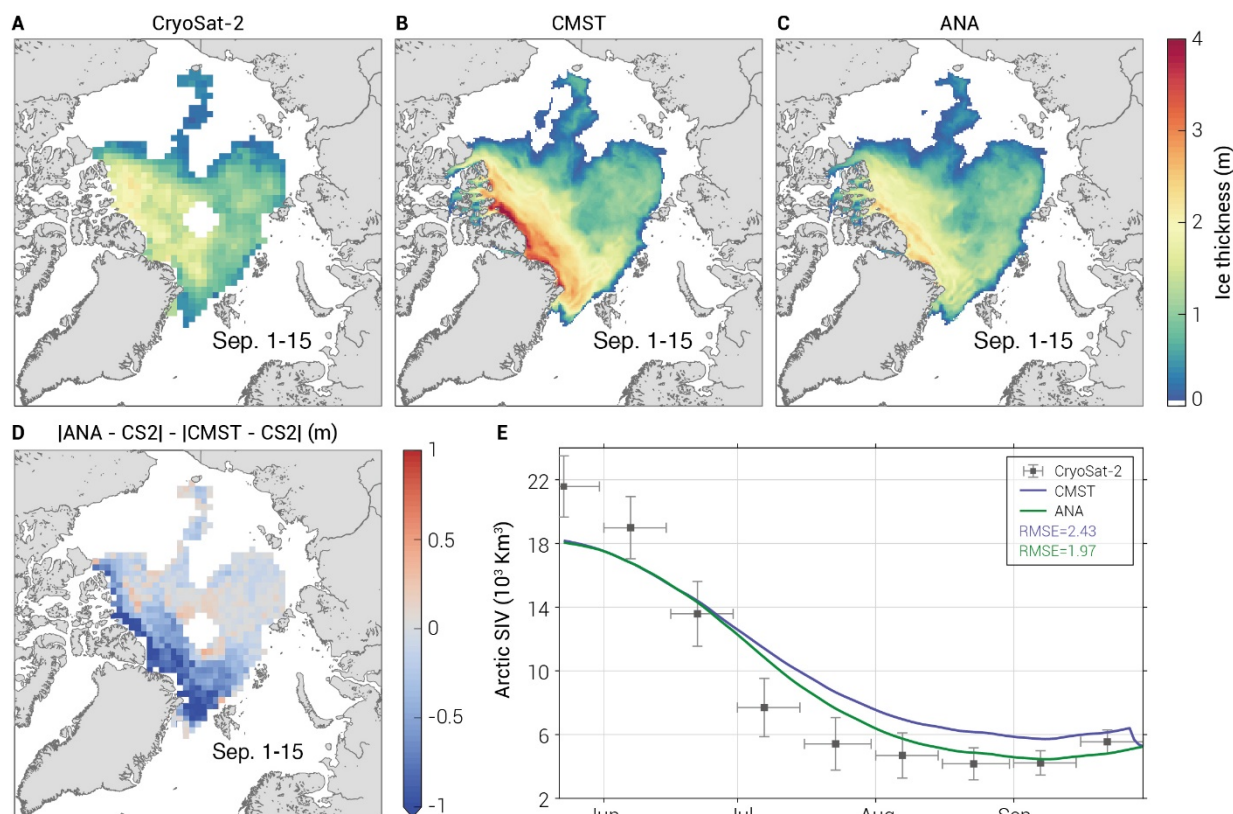
Fig. 4. Arctic sea-ice thickness (SIT) averaged over September 1−15, 2016, from CryoSat-2 (CS2), Combined Model and Satellite Thickness (CMST) and Analysis (ANA), shown in (a), (b) and (c), respectively. Panel (d) shows the difference between │ANA minus CS2│ and │CMST minus CS2│, which indicates the improvements obtained by assimilating CS2 SIT. Panel (e) presents the development of summer sea-ice volume (SIV) over time. The vertical bar in (e) for CryoSat-2 represents uncertainty, and the horizontal bar is the time span for biweekly CryoSat-2 data. Root-mean-square errors (RMSEs) for the CMST and ANA against the observations are shown in purple and green, respectively.

Because the sea-ice model parameterizations are imperfect and satellite measurements of ice thickness have significant uncertainties in coastal areas with thick, multiyear sea ice, the CMST analysis is most uncertain around the northern coast of the Canadian Arctic Archipelago and Greenland (Mu, Losch, et al., 2018). Comparisons between ANA, CMST, CryoSat-2, and airborne sea ice surveys are conducted to determine differences in certain places where strong sea ice deformation occurs. As shown in Fig. 5, CMST appears to estimate excessively thick ice in the survey regions, whereas CryoSat-2 measures thinner sea ice than do the airborne surveys, as shown in Landy et al. (2022). The median values of the airborne surveys, CMST and CryoSat-2 are 1.58 m, 2.33 m and 0.9 m, respectively. With a median of 1.86 m, which is closest to that of the airborne surveys, the ANA has the best agreement among CryoSat-2, CMST, and ANA. This result is also true for the dominating probability density estimates for the observed and simulated SIT. The best agreement between the airborne surveys and ANA is also verified by their lower and upper quartiles. Benefiting from the summer SIT assimilation and model dynamics, which implies that the satellite thickness measurements that are incompatible with the dynamics of the sea ice model are discarded in the data assimilation, the ANA reduces the overestimation of ice thickness obtained by the CMST, particularly in the Arctic Ocean north of Greenland, while preventing the underestimation evident in the CryoSat-2 observations.
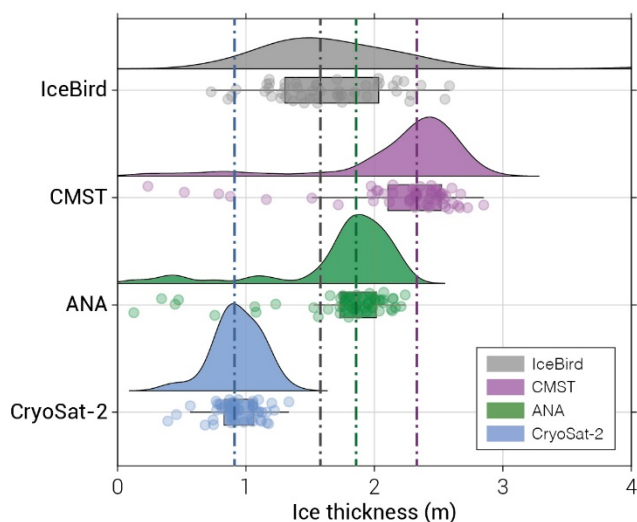
Fig. 5. Comparison between observed sea-ice thickness (SIT) from the airborne surveys (IceBird) and CryoSat-2 and the simulated SIT from the Combined Model and Satellite Thickness (CMST) and Analysis (ANA). The raincloud plots show the distributions of observed and simulated SIT and their key summary statistics (i.e., lower and upper quartiles, medians, and outliers). The medians for the IceBird observations, CMST, ANA and CryoSat-2 are represented by gray, purple, green and blue dashed lines, respectively. Translucent dots represent the observed and simulated SITs.

With sea-ice observations from the BGEP moorings, the performances of CryoSat-2, CMST and ANA are assessed in the Beaufort Sea (Fig. 6, Table 1 and Table A1). The three datasets replicate the SIT developments that were measured in situ (Figs. 6a-6c). Compared to the BGEP moorings, both the CMST and ANA show comparatively small RMSE and mean bias values. For the BGEP measurements, the RMSEs for ANA are up to 0.05 m smaller than those for CMST, while the mean bias is generally below 0.10 m and differs by up to 0.06 m, indicating that the further assimilation of CryoSat-2 improves not only the estimate of Arctic SIV but also the local SIT. Notably, the growth in SIT at the BGEP_B location during mid- to late September (Fig. 6b) is only well captured by ANA, which integrates model dynamics with satellite SIT.

Compared to the ADCPs (i.e., Vilk1-14 and Vilk3-14) deployed in the Laptev Sea, CryoSat-2, CMST and ANA have relatively larger deviations (Figs. 6d-6e). The RMSEs for ANA versus Vilk1-14 and Vilk3-14 are 0.61 m and 0.78 m, respectively, while the mean biases are −0.39 m and −0.43 m, respectively. Although the SIT as measured by ADCPs is underestimated by our model outputs, the mean bias for ANA is within the mean uncertainty (±0.96 m) of the ADCPs. Furthermore, the CryoSat-2 data show an even larger underestimation (Table A1). However, in contrast to the BGEP time series, the evolution of the SIT at the Vilk moorings is complex during the summer of 2016. The ice cover thickens between the start and end of the summer as highly deformed ice transited through the mooring locations (Belter et al., 2020). This demonstrates that ANA still functions better than CryoSat-2 data in the Laptev Sea.

Table 1. Main statistics [m] used to verify the sea-ice thickness of the Combined Model and Satellite Thickness (CMST) and Analysis (ANA) against in situ measurements (i.e., BGEP_A, BGEP_B, BGEP_D, Vilk1-14 and Vilk3-14) in summer 2016.

In situ observation	RMSE		Mean bias	
	CMST	ANA	CMST	ANA
BGEP_A	0.35	0.35	0.08	0.07
BGEP_B	0.24	0.23	0.01	−0.05
BGEP_D	0.40	0.35	0.09	0.03
Vilk1-14	0.61	0.61	−0.40	−0.39
Vilk3-14	0.76	0.78	−0.45	−0.43
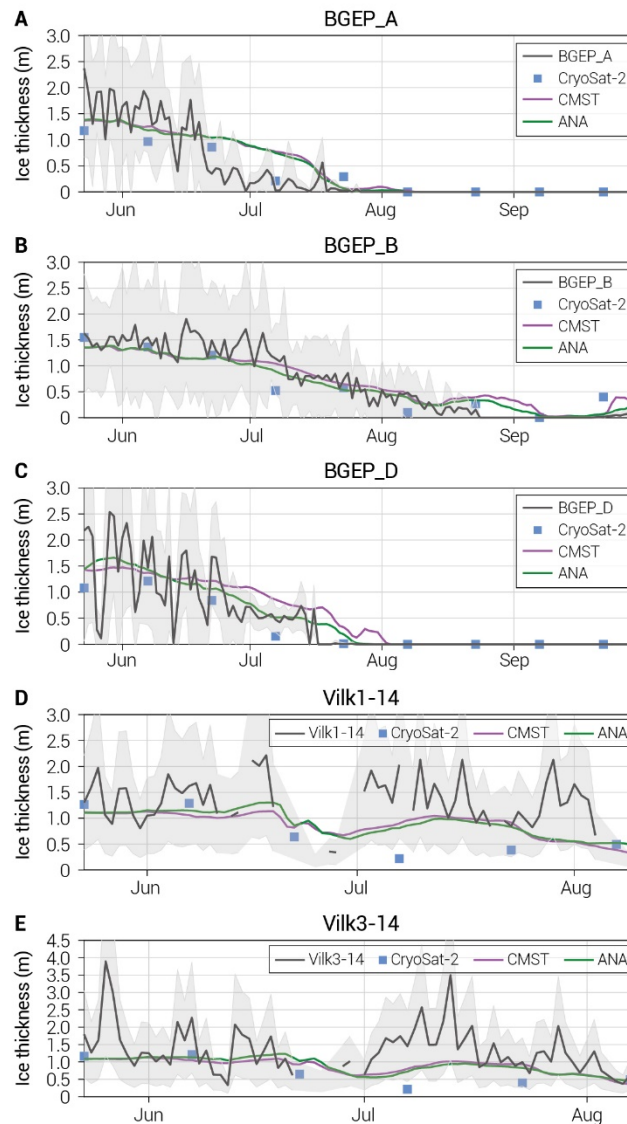
Fig. 6. Comparison of summer sea-ice thickness (SIT) from the Beaufort Gyre Exploration Program (BGEP) moorings, CryoSat-2, Combined Model and Satellite Thickness (CMST) and Analysis (ANA), during summer 2016. Panels (a, b and c) show the SIT developments

at BGEP_A, BGEP_B and BGEP_D, respectively. Panels (d) and (e) show the SIT developments at the acoustic Doppler current profiler (ADCP) sensor deployments (Vilk1-14 and Vilk3-14) in the Laptev Sea. Shaded areas indicate one standard deviation of uncertainty of the in situ observations.

4. Discussion

While the new CryoSat-2 summer SIT data represent a considerable improvement in satellite monitoring of Arctic sea ice, the SIT uncertainties are relatively larger in summer than in winter (Landy et al., 2022). These SIT uncertainties include uncertainties in the radar freeboard estimates introduced by the interaction of CryoSat-2 radar waves with snow overlying the sea ice (Nab et al., 2023). This is because the ability of radar waves to penetrate through snow to the ice surface varies depending on the salinity and roughness of the snow as well as changing snow properties in response to air temperatures and wind speed (Nab et al., 2023; Nandan et al., 2023). More importantly, for summer datasets, the interaction between melt ponds on the snow surface and CryoSat-2 radar waves is very poorly understood (Dawson et al., 2022).

To better estimate the Arctic summer SIT, we conduct a data assimilation experiment assimilating the recent CryoSat-2 summer SIT with an IAU approach. Even though our SIT estimates, which combine model dynamics and summer satellite SIT, are better than the CMST estimates, there are still uncertainties in the Laptev Sea. Because the Laptev Sea is a crucial sea area affecting navigation safety (e.g., Min et al., 2022; Min et al., 2023), model simulations need to be further optimized in years when sea ice conditions experience dramatic changes. Given that the snow depth uncertainties contribute a significant portion of the total radar-derived thickness uncertainty (Nab et al., 2023), the assimilation of snow depth has the potential to enhance sea-ice estimates (see, e.g., Kaminski et al. 2018). However, in Fritzner et al. (2019), assimilating snow depth led to a less accurate long-term estimate of SIE (Fritzner et al., 2019). Thus, making use of snow depth data requires further investigation (see Text S1 and Fig. S1 for discussion). Furthermore, the assimilation of sea ice drift data improves the thickness distribution (e.g., Rollenhagen et al., 2009), and assimilating sea surface temperature also improves simulations of sea ice edge and marginal SIT (e.g., Liang et al., 2019). Therefore, the multivariate assimilation of ice concentration, thickness, drift, snow depth, and sea surface temperature is expected to provide a more reliable estimate of Arctic sea ice.

Furthermore, accurate initialization of SIT has a significant impact on enhancing the model ability to forecast Arctic sea ice on seasonal time scales (e.g., Blanchard-Wrigglesworth et al., 2023; Day et al., 2014; Xiu et al., 2022) and is essential for the monthly timescale prediction of high-latitude atmospheric surface variables, such as the 2 m temperature (Day et al., 2014). Previous studies have shown the importance of incorporating SIT data from satellite observations and reanalysis into dynamic models for improving sea ice initial conditions (e.g., Allard et al., 2018; Dirkson et al., 2017; Fiedler et al., 2022; Mignac et al., 2022; Shu et al., 2021). For example, even though the ice thickness field was adjusted with SIT information from CryoSat-2 observations only once during the winter months, significant improvements in replicating SIT over multiyear ice have been found (Allard et al., 2018). Moreover, by assimilating satellite SIC and Pan-Arctic Ice-Ocean Modeling and Assimilation System (PIOMAS) SIT data, Shu et al. (2020) found that the forecast skill of Arctic summer sea ice was significantly improved and that the predicted integrated ice edge

error was reduced by approximately one order of magnitude; Collow et al. (2015) also revealed a significant improvement in predicting the extent of September Arctic sea ice, as well as an increase in interannual predictive skill. Compared with previous research, the CryoSat-2 summer SIT observations are incorporated into a coupled ice-ocean model for the first time, leading to significantly improved sea-ice estimates and initial conditions. Therefore, with the enhanced sea-ice initial states, our data assimilation system has the potential to improve sea-ice forecasts, particularly in summer, as evidenced by Yang et al. (2019).

5. Conclusion

The IAU method that is newly implemented in our system guarantees a gradual development of the sea-ice fields over time while allowing the assimilation of infrequent summer SIT data, which are only provided on a two-week basis, in conjunction with daily SIC data. Model dynamics play an important role in the assimilation, and the ANA thus has the potential to reduce the underestimation of SIT in satellite retrievals, especially in the Fram Strait and Arctic Ocean to northern Greenland (Landy et al., 2022), where the ice thermodynamically thickens and experiences deformation over many winter seasons (Kwok, 2015; Tschudi et al., 2016). Likewise, compared with airborne electromagnetic measurements of summer SIT, our ANA basically solves the overestimation of SIT estimated by CMST in those areas and thus provides a more reliable estimate of summer SIT. However, an increasing SIT toward the coast is also a common feature of sea ice dynamics. It is, therefore, difficult to conclude that the ANA is better than CMST for regions near the coast. Moreover, in comparison to the CMST reanalysis, which does not assimilate these summer SIT observations, the evolution of the SIV estimates agrees better with that derived from CryoSat-2.

These findings demonstrate the benefits of assimilating CryoSat-2 summer SIT for estimating Arctic sea ice and hence improving the initial states for sea-ice forecasts, which is highly relevant for marine navigation. Furthermore, our IAU assimilation scheme can be well applied to summer sea ice assimilation, which is important for developing a sea-ice reanalysis that assimilates the year-round satellite ice thickness and concentration. A continuous long-term ice thickness record with a finer temporal-spatial resolution that assimilates both the year-round SIC and SIT will be reconstructed in the future.

Data Availability: All data used in this study are openly accessible. The BGEP ULS-measured sea ice draft data were downloaded from https://www2.whoi.edu/site/beaufortgyre/data/mooring-data/. The sea-ice draft data measured by the AWI ADCP sensors were downloaded from https://doi.pangaea.de/10.1594/PANGAEA.912927. The SIC data provided by the National Snow and Ice Data Center and the University of Hamburg are available at https://nsidc.org/data/nsidc-0051/versions/2 and https://www.cen.uni-hamburg.de/en/icdc/data/, respectively. The UKMO ensemble forecasting data were obtained from the THORPEX Interactive Grand Global Ensemble (TIGGE) archive (https://apps.ecmwf.int/datasets/data/tigge/levtype=sfc/type=cf/). The CryoSat-2 SIT data are available from the British Antarctic Survey Polar Data Centre at https://doi.org/10.5285/D8C66670-57AD-44FC-8FEF-942A46734ECB. The MITgcm model code is available at http://mitgcm.org. The PDAF can be obtained from http://pdaf.awi.de.

References

Bailey, H., Hubbard, A., Klein, E. S., Mustonen, K.-R., Akers, P. D., Marttila, H., & Welker, J. M. (2021). Arctic sea-ice loss fuels extreme European snowfall. Nature Geoscience, 14(5), 283-288. https://doi.org/10.1038/s41561-021-00719-y

Belter, H. J., Krumpen, T., Hendricks, S., Hoelemann, J., Janout, M. A., Ricker, R., & Haas, C. (2020). Satellite-based sea ice thickness changes in the Laptev Sea from 2002 to 2017: comparison to mooring observations. The Cryosphere, 14(7), 2189-2203. https://doi.org/10.5194/tc-14-2189-2020

Belter, H. J., Krumpen, T., Janout, M. A., Ross, E., & Haas, C. (2021). An Adaptive Approach to Derive Sea Ice Draft from Upward-Looking Acoustic Doppler Current Profilers (ADCPs), Validated by Upward-Looking Sonar (ULS) Data. Remote Sensing, 13(21). https://doi.org/10.3390/rs13214335

Blockley, E. W., & Peterson, K. A. (2018). Improving Met Office seasonal predictions of Arctic sea ice using assimilation of CryoSat-2 thickness. The Cryosphere, 12(11), 3419-3438. https://doi.org/10.5194/tc-12-3419-2018

Bloom, S. C., Takacs, L. L., da Silva, A. M., & Ledvina, D. (1996). Data Assimilation Using Incremental Analysis Updates. Monthly Weather Review, 124(6), 1256-1271. https://doi.org/10.1175/1520-0493(1996)124<1256:DAUIAU>2.0.CO;2

Bowler, N. E., Arribas, A., Mylne, K. R., Robertson, K. B., & Beare, S. E. (2008). The MOGREPS short-range ensemble prediction system. Quarterly Journal of the Royal Meteorological Society, 134(632), 703-722. https://doi.org/10.1002/qj.234

Chylek, P., Folland, C., Klett, J. D., Wang, M., Hengartner, N., Lesins, G., & Dubey, M. K. (2022). Annual Mean Arctic Amplification 1970–2020: Observed and Simulated by CMIP6 Climate Models. Geophysical Research Letters, 49(13), e2022GL099371. https://doi.org/10.1029/2022GL099371

Cohen, J., Agel, L., Barlow, M., Garfinkel, C. I., & White, I. (2021). Linking Arctic variability and change with extreme winter weather in the United States. Science, 373(6559), 1116-1121. https://doi.org/10.1126/science.abi9167

Comiso, J. C., Cavalieri, D. J., Parkinson, C. L., & Gloersen, P. (1997). Passive microwave algorithms for sea ice concentration: A comparison of two techniques. Remote Sensing of Environment, 60(3), 357-384. https://doi.org/10.1016/S0034-4257(96)00220-9

Dawson, G., Landy, J., Tsamados, M., Komarov, A. S., Howell, S., Heorton, H., & Krumpen, T. (2022). A 10-year record of Arctic summer sea ice freeboard from CryoSat-2. Remote Sensing of Environment, 268, 112744. https://doi.org/10.1016/j.rse.2021.112744

Day, J. J., Hawkins, E., & Tietsche, S. (2014). Will Arctic sea ice thickness initialization improve seasonal forecast skill? Geophysical Research Letters, 41(21), 7566-7575. https://doi.org/10.1002/2014GL061694

DiGirolamo, N., Parkinson, C. L., Cavalieri, D. J., Gloersen, P., & Zwally, H. J. (2022). Sea Ice Concentrations from Nimbus-7 SMMR and DMSP SSM/I-SSMIS Passive Microwave Data, Version 2 [Data Set], Boulder, Colorado USA. NASA National Snow and Ice Data Center Distributed Active Archive Center. https://doi.org/10.5067/MPYG15WAA4WX.

Eicken, H. (2013). Arctic sea ice needs better forecasts. Nature, 497(7450), 431-433. https://doi.org/10.1038/497431a

Farrell, S. L., Duncan, K., Buckley, E. M., Richter-Menge, J., & Li, R. (2020). Mapping Sea Ice Surface Topography in High Fidelity With ICESat-2. Geophysical Research Letters, 47(21), e2020GL090708. https://doi.org/10.1029/2020GL090708

Gaspari, G., & Cohn, S. E. (1999). Construction of correlation functions in two and three dimensions. Quarterly Journal of the Royal Meteorological Society, 125(554), 723-757. https://doi.org/10.1002/qj.49712555417

Hibler, W. D. (1979). A Dynamic Thermodynamic Sea Ice Model. Journal of Physical Oceanography, 9(4), 815-846. https://doi.org/10.1175/1520-0485(1979)009<0815:ADTSIM>2.0.CO;2

Kaleschke, L., Tian-Kunze, X., Maaß, N., Mäkynen, M., & Drusch, M. (2012). Sea ice thickness retrieval from SMOS brightness temperatures during the Arctic freeze-up period. Geophysical Research Letters, 39(5). https://doi.org/10.1029/2012GL050916

Kaleschke, L., Lupkes, C., Vihma, T., Haarpaintner, J., Bochert, A., Hartmann, J., & Heygster, G. (2001). SSM/I sea ice remote sensing for mesoscale ocean-atmosphere interaction analysis. Canadian Journal of Remote Sensing, 27(5), 526-537. https://doi.org/10.1080/07038992.2001.10854892

Kaminski, T., Kauker, F., Toudal Pedersen, L., Voßbeck, M., Haak, H., Niederdrenk, L., et al. (2018). Arctic Mission Benefit Analysis: impact of sea ice thickness, freeboard, and snow depth products on sea ice forecast performance. The Cryosphere, 12(8), 2569-2594. https://doi.org/10.5194/tc-12-2569-2018

Kern, S., Kaleschke, L., & Spreen, G. (2010). Climatology of the Nordic (Irminger, Greenland, Barents, Kara and White/Pechora) Seas ice cover based on 85 GHz satellite microwave radiometry: 1992–2008. Tellus A: Dynamic Meteorology and Oceanography, 62(4), 411-434. https://doi.org/10.1111/j.1600-0870.2010.00457.x

Krumpen, T., Belter, H. J., Boetius, A., Damm, E., Haas, C., Hendricks, S., et al. (2019). Arctic warming interrupts the Transpolar Drift and affects long-range transport of sea ice and ice-rafted matter. Scientific Reports, 9(1), 5459. https://doi.org/10.1038/s41598-019-41456-y

Krumpen, T., Birrien, F., Kauker, F., Rackow, T., von Albedyll, L., Angelopoulos, M., et al. (2020). The MOSAiC ice floe: sediment-laden survivor from the Siberian shelf. The Cryosphere, 14(7), 2173-2187. https://doi.org/10.5194/tc-14-2173-2020

Kwok, R. (2015). Sea ice convergence along the Arctic coasts of Greenland and the Canadian Arctic Archipelago: Variability and extremes (1992–2014). Geophysical Research Letters, 42(18), 7598-7605. https://doi.org/10.1002/2015GL065462

Kwok, R. (2018). Arctic sea ice thickness, volume, and multiyear ice coverage: losses and coupled variability (1958–2018). Environmental Research Letters, 13(10), 105005. https://doi.org/10.1088/1748-9326/aae3ec

Landy, J. C., Tsamados, M., & Scharien, R. K. (2019). A Facet-Based Numerical Model for Simulating SAR Altimeter Echoes From Heterogeneous Sea Ice Surfaces. IEEE Transactions on Geoscience and Remote Sensing, 57(7), 4164-4180. https://doi.org/10.1109/TGRS.2018.2889763

Landy, J. C., Petty, A. A., Tsamados, M., & Stroeve, J. C. (2020). Sea Ice Roughness Overlooked as a Key Source of Uncertainty in CryoSat-2 Ice Freeboard Retrievals. Journal of Geophysical Research: Oceans, 125(5), e2019JC015820. https://doi.org/10.1029/2019JC015820

Landy, J. C., Dawson, G. J., Tsamados, M., Bushuk, M., Stroeve, J. C., Howell, S. E. L., et al. (2022). A year-round satellite sea-ice thickness record from CryoSat-2. Nature. https://doi.org/10.1038/s41586-022-05058-5

Lavergne, T., Sørensen, A. M., Kern, S., Tonboe, R., Notz, D., Aaboe, S., et al. (2019). Version 2 of the EUMETSAT OSI SAF and ESA CCI sea-ice concentration climate data records. The Cryosphere, 13(1), 49-78. https://doi.org/10.5194/tc-13-49-2019

Lawrence, I. R., Armitage, T. W. K., Tsamados, M. C., Stroeve, J. C., Dinardo, S., Ridout, A. L., et al. (2021). Extending the Arctic sea ice freeboard and sea level record with the Sentinel-3 radar altimeters. Advances in Space Research, 68(2), 711-723. https://doi.org/10.1016/j.asr.2019.10.011

Laxon, S. W., Giles, K. A., Ridout, A. L., Wingham, D. J., Willatt, R., Cullen, R., et al. (2013). CryoSat-2 estimates of Arctic sea ice thickness and volume. Geophysical Research Letters, 40(4), 732-737. https://doi.org/10.1002/grl.50193

Lellouche, J. M., Le Galloudec, O., Drévillon, M., Régnier, C., Greiner, E., Garric, G., et al. (2013). Evaluation of global monitoring and forecasting systems at Mercator Océan. Ocean Sci., 9(1), 57-81. https://doi.org/10.5194/os-9-57-2013

Li, X., Yang, Q., Yu, L., Holland, P. R., Min, C., Mu, L., & Chen, D. (2022). Unprecedented Arctic sea ice thickness loss and multiyear-ice volume export through Fram Strait during 2010–2011. Environmental Research Letters, 17(9), 095008. https://doi.org/10.1088/1748-9326/ac8be7

Liang, X., Losch, M., Nerger, L., Mu, L., Yang, Q., & Liu, C. (2019). Using Sea Surface Temperature Observations to Constrain Upper Ocean Properties in an Arctic Sea Ice-Ocean Data Assimilation System. Journal of Geophysical Research: Oceans, 124(7), 4727-4743. https://doi.org/10.1029/2019JC015073

Liu, J., Song, M., Zhu, Z., Horton, R. M., Hu, Y., & Xie, S.-P. (2022). Arctic sea-ice loss is projected to lead to more frequent strong El Niño events. Nature Communications, 13(1), 4952. https://doi.org/10.1038/s41467-022-32705-2

Liston, G. E., Stroeve, J., & Itkin., P. (2021). Lagrangian Snow Distributions for Sea-Ice Applications, Version 1 [Data Set]. Boulder, Colorado USA. NASA National Snow and Ice Data Center Distributed Active Archive Center. https://doi.org/10.5067/27A0P5M6LZBI

Losch, M., Menemenlis, D., Campin, J.-M., Heimbach, P., & Hill, C. (2010). On the formulation of sea-ice models. Part 1: Effects of different solver implementations and parameterizations. Ocean Modelling, 33(1), 129-144. https://doi.org/10.1016/j.ocemod.2009.12.008

Marshall, J., Adcroft, A., Hill, C., Perelman, L., & Heisey, C. (1997). A finite-volume, incompressible Navier Stokes model for studies of the ocean on parallel computers. Journal of Geophysical Research: Oceans, 102(C3), 5753-5766. https://doi.org/10.1029/96JC02775

Massonnet, F., Fichefet, T., & Goosse, H. (2015). Prospects for improved seasonal Arctic sea ice predictions from multivariate data assimilation. Ocean Modelling, 88, 16-25. https://doi.org/10.1016/j.ocemod.2014.12.013

Melling, H., Johnston, P. H., & Riedel, D. A. (1995). Measurements of the Underside Topography of Sea-Ice by Moored Subsea Sonar. Journal of Atmospheric and Oceanic Technology, 12(3), 589-602. https://doi.org/10.1175/1520-0426(1995)012<0589:MOTUTO>2.0.CO;2

Mignac, D., Martin, M., Fiedler, E., Blockley, E., & Fournier, N. (2022). Improving the Met Office's Forecast Ocean Assimilation Model (FOAM) with the assimilation of satellite-derived sea-ice thickness data from CryoSat-2 and SMOS in the Arctic. Quarterly Journal of the Royal Meteorological Society, 148(744), 1144-1167. https://doi.org/10.1002/qj.4252

Min, C., Mu, L., Yang, Q., Ricker, R., Shi, Q., Han, B., et al. (2019). Sea ice export through the Fram Strait derived from a combined model and satellite data set. The Cryosphere, 13(12), 3209-3224. https://doi.org/10.5194/tc-13-3209-2019

Min, C., Yang, Q., Mu, L., Kauker, F., & Ricker, R. (2021). Ensemble-based estimation of sea-ice volume variations in the Baffin Bay. The Cryosphere, 15(1), 169-181. https://doi.org/10.5194/tc-15-169-2021

Min, C., Yang, Q., Chen, D., Yang, Y., Zhou, X., Shu, Q., & Liu, J. (2022). The Emerging Arctic Shipping Corridors. Geophysical Research Letters, 49(10), e2022GL099157. https://doi.org/10.1029/2022GL099157

Min, C., Zhou, X., Luo, H., Yang, Y., Wang, Y., Zhang, J., & Yang, Q. (2023). Toward Quantifying the Increasing Accessibility of the Arctic Northeast Passage in the Past Four Decades. Advances in Atmospheric Sciences. https://doi.org/10.1007/s00376-022-2040-3

Mu, L., Losch, M., Yang, Q., Ricker, R., Losa, S. N., & Nerger, L. (2018). Arctic-Wide Sea Ice Thickness Estimates From Combining Satellite Remote Sensing Data and a Dynamic Ice-Ocean Model with Data Assimilation During the CryoSat-2 Period. Journal of Geophysical Research: Oceans, 123(11), 7763-7780. https://doi.org/10.1029/2018JC014316

Mu, L., Yang, Q., Losch, M., Losa, S. N., Ricker, R., Nerger, L., & Liang, X. (2018). Improving sea ice thickness estimates by assimilating CryoSat-2 and SMOS sea ice thickness data simultaneously. Quarterly Journal of the Royal Meteorological Society, 144(711), 529-538. https://doi.org/10.1002/qj.3225

Nab, C., Mallett, R., Gregory, W., Landy, J., Lawrence, I., Willatt, R., et al. (2023). Synoptic Variability in Satellite Altimeter-Derived Radar Freeboard of Arctic Sea Ice. Geophysical Research Letters, 50(2), e2022GL100696. https://doi.org/10.1029/2022GL100696

Nandan, V., Willatt, R., Mallett, R., Stroeve, J., Geldsetzer, T., Scharien, R., et al. (2023). Wind redistribution of snow impacts the Ka- and Ku-band radar signatures of Arctic sea ice. The Cryosphere, 17(6), 2211-2229. https://doi.org/10.5194/tc-17-2211-2023

Nerger, L., & Hiller, W. (2013). Software for ensemble-based data assimilation systems—Implementation strategies and scalability. Computers & Geosciences, 55, 110-118. https://doi.org/10.1016/j.cageo.2012.03.026

Nerger, L., Janjić, T., Schröter, J., & Hiller, W. (2012). A Unification of Ensemble Square Root Kalman Filters. Monthly Weather Review, 140(7), 2335-2345. https://doi.org/10.1175/MWR-D-11-00102.1

Nguyen, A. T., Menemenlis, D., & Kwok, R. (2011). Arctic ice-ocean simulation with optimized model parameters: Approach and assessment. Journal of Geophysical Research-Oceans, 116. https://doi.org/10.1029/2010JC006573

Ourmières, Y., Brankart, J. M., Berline, L., Brasseur, P., & Verron, J. (2006). Incremental Analysis Update Implementation into a Sequential Ocean Data Assimilation System. Journal of Atmospheric and Oceanic Technology, 23(12), 1729-1744. https://doi.org/10.1175/JTECH1947.1

Park, Y. Y., Buizza, R., & Leutbecher, M. (2008). TIGGE: Preliminary results on comparing and combining ensembles. Quarterly Journal of the Royal Meteorological Society, 134(637), 2029-2050. https://doi.org/10.1002/qj.334

Parkinson, C. L., & Washington, W. M. (1979). A large-scale numerical model of sea ice. Journal of Geophysical Research: Oceans, 84(C1), 311-337. https://doi.org/10.1029/JC084iC01p00311

Petty, A. A., Stroeve, J. C., Holland, P. R., Boisvert, L. N., Bliss, A. C., Kimura, N., & Meier, W. N. (2018). The Arctic sea ice cover of 2016: a year of record-low highs and higher-than-expected lows. The Cryosphere, 12(2), 433-452. https://doi.org/10.5194/tc-12-433-2018

Petty, A. A., Schröder, D., Stroeve, J. C., Markus, T., Miller, J., Kurtz, N. T., et al. (2017). Skillful spring forecasts of September Arctic sea ice extent using passive microwave sea ice observations. Earth's Future, 5(2), 254-263. https://doi.org/10.1002/2016EF000495

Pfaffling, A., Haas, C., & Reid, J. E. (2007). Direct helicopter EM - Sea-ice thickness inversion assessed with synthetic and field data. Geophysics, 72(4), F127-F137. https://doi.org/10.1190/1.2732551

Qi, D., Ouyang, Z., Chen, L., Wu, Y., Lei, R., Chen, B., et al. (2022). Climate change drives rapid decadal acidification in the Arctic Ocean from 1994 to 2020. Science, 377(6614), 1544-1550. https://doi.org/10.1126/science.abo0383

Rantanen, M., Karpechko, A. Y., Lipponen, A., Nordling, K., Hyvärinen, O., Ruosteenoja, K., et al. (2022). The Arctic has warmed nearly four times faster than the globe since 1979. Communications Earth & Environment, 3(1), 168. https://doi.org/10.1038/s43247-022-00498-3

Ricker, R., Hendricks, S., Helm, V., Skourup, H., & Davidson, M. (2014). Sensitivity of CryoSat-2 Arctic sea-ice freeboard and thickness on radar-waveform interpretation. The Cryosphere, 8(4), 1607-1622. https://doi.org/10.5194/tc-8-1607-2014

Rollenhagen, K., Timmermann, R., Janjić, T., Schröter, J., & Danilov, S. (2009). Assimilation of sea ice motion in a finite-element sea ice model. Journal of Geophysical Research: Oceans, 114(C5). https://doi.org/10.1029/2008JC005067

Semtner, A. J. (1976). A Model for the Thermodynamic Growth of Sea Ice in Numerical Investigations of Climate. Journal of Physical Oceanography, 6(3), 379-389. https://doi.org/10.1175/1520-0485(1976)006<0379:AMFTTG>2.0.CO;2

Spreen, G., Kaleschke, L., & Heygster, G. (2008). Sea ice remote sensing using AMSR-E 89-GHz channels. Journal of Geophysical Research: Oceans, 113(C2). https://doi.org/10.1029/2005JC003384

Stroeve, J., Liston, G. E., Buzzard, S., Zhou, L., Mallett, R., Barrett, A., et al. (2020). A Lagrangian snow evolution system for sea ice applications (SnowModel-LG): Part II—Analyses. Journal of Geophysical Research: Oceans, 125, e2019JC015900. https://doi.org/10.1029/2019JC015900

Stroeve, J., & Notz, D. (2018). Changing state of Arctic sea ice across all seasons. Environmental Research Letters, 13(10), 103001. https://doi.org/10.1088/1748-9326/aade56

Tian-Kunze, X., Kaleschke, L., Maaß, N., Mäkynen, M., Serra, N., Drusch, M., & Krumpen, T. (2014). SMOS-derived thin sea ice thickness: algorithm baseline, product specifications and initial verification. The Cryosphere, 8(3), 997-1018. https://doi.org/10.5194/tc-8-997-2014

Xie, J., Counillon, F., & Bertino, L. (2018). Impact of assimilating a merged sea-ice thickness from CryoSat-2 and SMOS in the Arctic reanalysis. The Cryosphere, 12(11), 3671-3691. https://doi.org/10.5194/tc-12-3671-2018

Yang, Q., Losa, S. N., Losch, M., Jung, T., & Nerger, L. (2015). The role of atmospheric uncertainty in Arctic summer sea ice data assimilation and prediction. Quarterly Journal of the Royal Meteorological Society, 141(691), 2314-2323. https://doi.org/10.1002/qj.2523

Yang, Q., Mu, L., Wu, X., Liu, J., Zheng, F., Zhang, J., & Li, C. (2019). Improving Arctic sea ice seasonal outlook by ensemble prediction using an ice-ocean model. Atmospheric Research, 227, 14-23. https://doi.org/10.1016/j.atmosres.2019.04.021

Yang, Q., Losch, M., Losa, S. N., Jung, T., Nerger, L., & Lavergne, T. (2016). Brief communication: The challenge and benefit of using sea ice concentration satellite data products with uncertainty estimates in summer sea ice data assimilation. The Cryosphere, 10(2), 761-774. https://doi.org/10.5194/tc-10-761-2016

Yang, Q., Losa, S. N., Losch, M., Tian-Kunze, X., Nerger, L., Liu, J., et al. (2014). Assimilating SMOS sea ice thickness into a coupled ice-ocean model using a local SEIK filter. Journal of Geophysical Research: Oceans, 119(10), 6680-6692. https://doi.org/10.1002/2014JC009963

Zhang, J., & Hibler, W. D. (1997). On an efficient numerical method for modeling sea ice dynamics. Journal of Geophysical Research: Oceans, 102(C4), 8691-8702. https://doi.org/10.1029/96JC03744

Zhou, X., Min, C., Yang, Y., Landy, J. C., Mu, L., & Yang, Q. (2021). Revisiting Trans-Arctic Maritime Navigability in 2011–2016 from the Perspective of Sea Ice Thickness. Remote Sensing, 13(14), 2766. https://doi.org/10.3390/rs13142766

Appendix A

In this Appendix, Fig. A1 shows the sea ice volume (SIV) development in summer 2016. We describe how we calculated the statistics that are used to assess sea ice estimates and satellite observations. The comparison of the Arctic sea-ice extents (SIEs) from the Analysis (ANA), CMST and reference sea-ice concentration observations are presented in Fig. A2. Additionally, the main statistics used to verify the sea-ice thickness of CryoSat-2 data against in situ measurements are shown in Table A1.
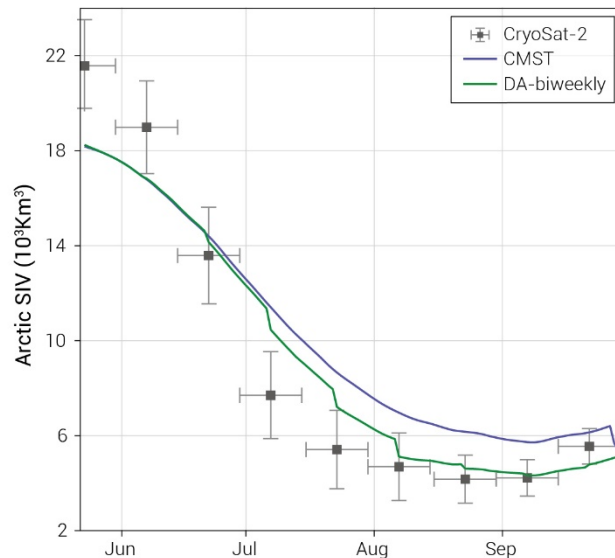
A1 Sea-ice volume development

Fig. A1. Sea ice volume (SIV) development in summer 2016. SIV as determined by the Combined Model and Satellite Thickness (CMST) reanalysis is represented by the purple line. The green line (DA-biweekly) represents the evolution of the SIV based on sea ice estimates that directly assimilate daily sea ice concentration and biweekly CryoSat-2 sea ice thickness. The vertical bar for CryoSat-2 is for uncertainty, and the horizontal bar is the time span for biweekly CryoSat-2 data.

A2 Statistics used to verify the sea ice estimates and CryoSat-2 observations

To verify the sea-ice estimates conducted by our data assimilation system and CryoSat-2 observations, the root-mean-square error (RMSE), mean bias (MB) and correlation coefficient (CC) are calculated as follows:

$$RMSE = \sqrt{\frac{\Sigma(M - OBS)^2}{n}}, \qquad (1)$$

$$MB = \frac{\Sigma(M - OBS)}{n}, \qquad (2)$$

$$CC = \frac{cov(M, OBS)}{\sigma_M \sigma_{OBS}}, \qquad (3)$$

where M represents the model outputs (both CMST and Analysis) and CryoSat-2 SIT, OBS represents the SIT observations, and n is used to calculate the number of observations. The covariance operator and standard deviation are represented by cov and σ, respectively.

A3 Sea-ice extent from sea-ice estimates and observations

The correlation coefficients for the SIE between the ANA/CMST and observations are nearly equal. Statistically, the correlation coefficient for the SIE between ANA and NSIDC data is ~1. The RMSE for the SIE calculated from the ANA and observations is approximately 0.72×10^6 km^2, while it is somewhat larger when calculated using the CMST and observations, at 0.74×10^6 km^2, demonstrating that the ANA slightly improves the SIE estimation.
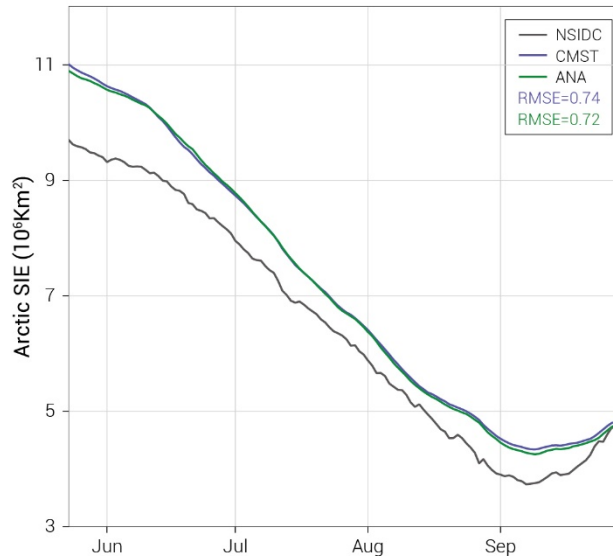

Fig. A2. The developments of summer sea-ice extent (SIE) calculated from NSIDC sea-ice observations, Combined Model and Satellite Thickness (CMST) and Analysis (ANA). The root-mean-square errors (RMSEs) for the CMST against the observations and the ANA against the observations are shown in purple and green, respectively.

A4 Evaluation of CryoSat-2 summer observations

Table A1. Main statistics [m] used to verify the sea-ice thickness of CryoSat-2 data against in situ measurements (i.e., BGEP_A, BGEP_B, BGEP_D, Vilk1-14 and Vilk3-14) in summer 2016. Notably, the in situ observations are averaged to the biweekly mean, whose duration corresponds to the biweekly data from CryoSat-2.

In situ observation	RMSE	Mean bias
BGEP_A	0.26	−0.06
BGEP_B	0.25	−0.06
BGEP_D	0.22	−0.13
Vilk1-14	0.71	−0.57
Vilk3-14	0.76	−0.61